

Fabrication and characterization of MSM photodetector based on DC sputtered CuO film

SADOON FARRUKH^a, NAVEED AFZAL^{a,*}, ANAS A. AHMED^b, MOHSIN RAFIQUE^a, MUHAMMAD AKRAM RAZA^c

^aCentre for Advanced Studies in Physics, GC University, Lahore, Pakistan

^bSchool of Physics, Universiti Sains, Malaysia, Malaysia

^cCentre of Excellence in Solid State Physics, University of the Punjab, Lahore, Pakistan

Copper Oxide film of monoclinic phase was deposited on silicon substrate by DC magnetron sputtering. A metal-semiconductor-metal (MSM) photodetector was fabricated by developing two interdigitated Ni electrodes on the film. The current-voltage characteristics of Ni/CuO/Ni device revealed Schottky contact formation which was attributed to Fermi-level pinning at the metal-semiconductor interface. The photo-response of the device was recorded by exposing it to the light of different wavelengths (850, 505, 405 and 365 nm). The results showed a significant increase in current under 505 nm light exposure. The Schottky barrier height was reduced after exposing the device to light.

(Received March 17, 2021; accepted November 24, 2021)

Keywords: Copper oxide, MSM photodiode, Sensitivity, Response time

1. Introduction

Copper oxide is a well-known p-type semiconductor that is widely recognized due to its good electrical properties, high optical absorption coefficient, non-toxicity and abundance [1-2]. Such characteristics of copper oxide offer potential applications in optoelectronic devices, batteries, photo-catalyst, and gas sensors [3-7]. Copper oxide exhibits three different phases such as CuO, Cu₂O and Cu₄O₃ [8]. The CuO is cupric oxide, having a band gap between 1.3 to 2.10 eV. The Cu₂O is a cuprous oxide phase which has a band gap in the range of 2.10 to 2.61 eV. The Cu₄O₃ is known as a paramelaconite phase whose properties are similar to the cupric oxide phase [8-10]. Copper oxide has been synthesized by different techniques, like chemical vapor deposition, chemical bath deposition, thermal oxidation, sol-gel spin coating, spray pyrolysis, electro-deposition, direct current (DC) and radiofrequency (RF) magnetron sputtering [11-20]. The sputter deposition technique possesses an advantage over the other methods in terms of high deposition rate, large area coating on substrate, controllability, and uniformity of film thickness and composition. However, the phases and physical properties of the sputtered copper oxide film depend upon the deposition parameters such as oxygen pressure, sputtering power, substrate temperature, and target-substrate distance [21-22].

Currently, copper oxide based visible light photodetectors have gained attention from researchers due to a potential capability of copper oxide film to absorb the visible light, high mechanical stability and easy processing [23-24]. These photodetectors find a wide range of applications, such as in optical communications, environmental research, imaging, and chemical analysis.

The visible light detectors made up of copper oxide exhibit high optical absorption in the visible range as compared to Si-based photodetectors, which are bulky and made up of a brittle material [24]. However, only a few studies have been conducted so far on the fabrication of copper oxide based photodetectors [25-27]. In these studies, the copper oxide film based heterojunction photodetectors were reported.

A metal-semiconductor-metal (MSM) photodetector is a type of photodetector that can be easily fabricated due to its simple structure. Also it displays fast response and high current gain as compared to the heterojunction photodetectors [28]. Previously, only a few studies have reported the fabrication of copper oxide based MSM photodetectors [24, 29]. Raghavendra *et al.* [29] designed CuO MSM visible photodetector on quartz substrate by depositing silver (Ag) contacts on the CuO film. The device exhibited low responsivity values of 0.33 and 0.59 mA/W for blue and red lights respectively. Furthermore, an increase in photocurrent was not significant under visible light exposure. Recent studies have shown that the crystallinity of metal oxide thin films such as CuO, NiO, V₂O₅ etc. on silicon is better than that on the glass substrate which is amorphous in nature [30-32]. The high crystallinity of a thin film helps in improving its photodetection properties due to reduction of structural defects [33-34]. In this work, a cupric oxide photodetector was fabricated on Si (100) with two interdigitated nickel (Ni) electrodes and its photodetection characteristics were investigated.

2. Methodology

The Si (100) was used for the deposition of the copper oxide film. A sample of 2.0 x 1.0 cm² dimension was cleaned using acetone and then dried. The DC magnetron sputtering system (DaON 1000S) was employed for the synthesis of the copper oxide film. The copper target was fixed on a holder inside the sputtering chamber, and the Si sample was adjusted above in front of the target. The sputtering chamber was evacuated up to 3 x 10⁻⁵ mbar using rotary and turbo molecular pumps to eliminate the contaminated gases. Then, the chamber was filled with argon and oxygen gasses with a ratio of 90:10, respectively and the deposition pressure was maintained at 1 x 10⁻³ mbar. Then, pure copper was sputtered by applying DC voltage at room temperature. The detail of the film's deposition parameters is given in Table 1. The film deposited on Si was characterized by X-ray diffraction (XRD), field emission scanning electron microscope (FESEM) and ultraviolet-visible spectroscopy for the investigation of structural, morphological and optical properties. The copper oxide based MSM photodetector was fabricated by depositing two interdigitated electrodes of Ni on the film by thermal evaporator system [35]. A finger metal mask was used for this purpose. The Ni was thermally evaporated on the film under a high vacuum. The schematic diagram of Ni/CuO/Ni MSM photodetector set up is shown in Fig. 1. The Keithly-2400 system was used to study the current-voltage (I-V) and current-time (I-t) characteristics of the device.

Table 1 Sputter deposition parameters of CuO film

Deposition parameters	Values
Base pressure	2.3 x 10 ⁻⁵ mbar
Working pressure	1 x 10 ⁻³ mbar
Ar:O ₂	90:10
Voltage	350
Current	120 mA
Power	30 W
Sputtering time	1 hour 20 minutes
Film Thickness	~350 nm

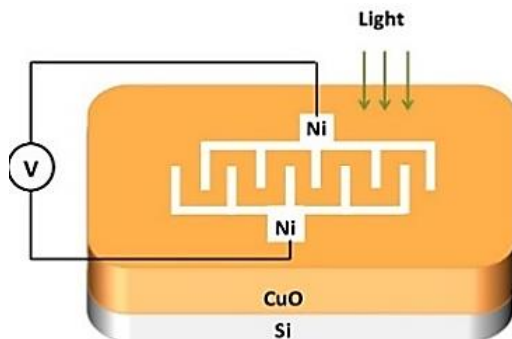


Fig. 1. Schematic diagram of Ni/CuO/Ni photodetector (color online)

3. Results and discussion

The XRD pattern of copper oxide film on silicon is shown in Fig. 2. The formation of CuO peak at 35.5° corresponding to (-111) plane indicates the monoclinic nature of the film (JCPDS card number 48-1548). Besides, the Si (100) peak appears at 69.5° showing a reflection from the substrate. None of Cu₂O and Cu₄O₃ peak is visible in the XRD pattern which illustrates that the copper oxide film on silicon exhibits only a CuO phase having monoclinic crystal structure.

The crystallite size of CuO (-111) film (D) was calculated by using Debye Scherer's formula as follows [35];

$$D = \frac{k\lambda}{\beta \cos\theta} \quad (1)$$

Here 'k' represents the shape constant (having value 0.9), 'θ' is Bragg's angle and 'β' indicates full width at half maximum of CuO diffraction peak. The crystallite size was found to be 13.9 nm.

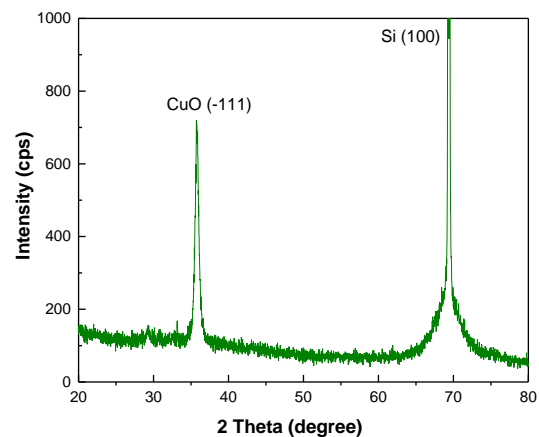


Fig. 2. X-ray diffraction graph of CuO film synthesized on Si (100) (color online)

Fig. 3 shows the FESEM image of the CuO film. The surface morphology of CuO is taken at a scale of 500 nm with a magnification of 100,000X. The surface morphology indicates the formation of small interconnected grains of the copper oxide film forming a dense structure. The average grain size of CuO was found to be 15 nm. This value is in close agreement with the crystallite size calculated through XRD.

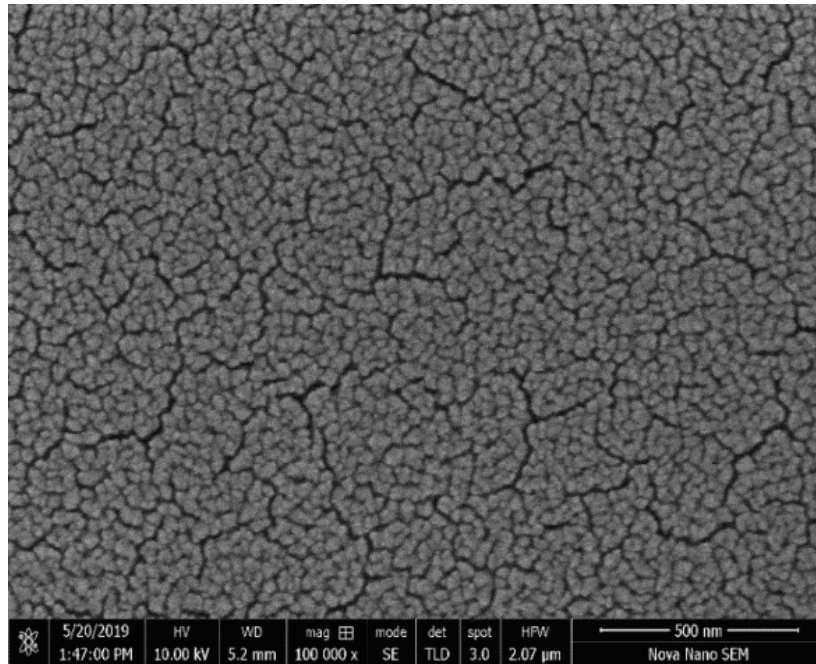


Fig. 3. FESEM Image of copper oxide film

The band gap of the copper oxide film was evaluated from the UV-Vis reflectance spectrum as shown in Fig. 4. A high percentage of reflectance is observed in the infrared region, whereas the reflectance decreases with decreasing the wavelength towards the visible region. When UV light falls on the copper oxide film, then some portion of this light is reflected from the film, and the other part is transmitted in the film and reflects from the silicon substrate. The two reflected light rays combine to produce interference fringes. These interference fringes are disappeared when the light is absorbed by the film [35-37]. The wavelength at which this absorption takes place is called cut off wavelength. The absorption edge is found at 512 nm from the reflectance graph. This corresponds to energy band gap of 2.42 eV as obtained from the following equation;

$$E = \frac{hc}{\lambda_{\text{cutoff}}} \quad (2)$$

Here 'h' is Planks constant, c is the speed of light and λ_{cutoff} is the wavelength that corresponds to the absorption edge. The energy band gap obtained in this study is higher than the band gap energy reported for the bulk CuO in the literature (1.2 eV). This higher value can be attributed to the quantum confinement effect which occurs because of the small crystallite size of the nanomaterial [29, 38-39]. In this study, the crystallite size of CuO (13.9 nm) is in the range of the Bohr exciton radius (6.6 to 28.7 nm), therefore the smaller crystallite size of the nanomaterial affects its energy band gap. A decrease in crystallite size reduces the number of atoms in it which causes a decrease in the number of overlapping orbitals. Owing to this reason, the energy gap between the valence and conduction bands increases [38]. The higher band gap value of CuO in this work is in good

agreement with the previous studies dealing with the nanocrystalline CuO film [38-39].

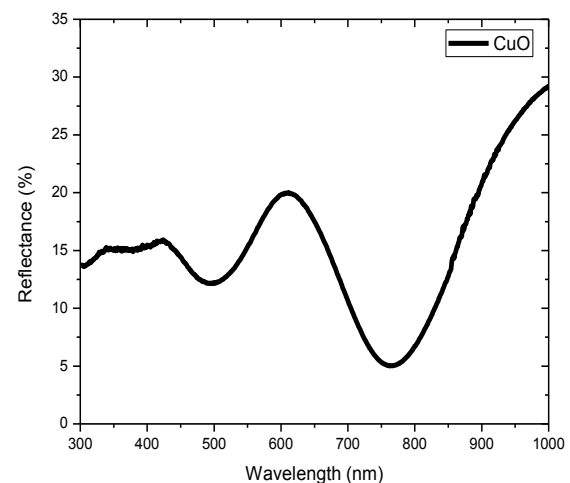


Fig. 4. UV-vis spectroscopy of CuO film

The current versus voltage graphs of Ni/CuO/Ni MSM photodetector were taken in the absence and presence of various lights wavelengths ranging from ultraviolet to infrared region (365, 405, 505, and 805 nm) (Fig. 5). The figure shows that both the dark and photocurrent curves almost overlap on each other at 365 and 405 nm, indicating no difference between the dark and photocurrent values. However, at 505 nm, a significant increase in the photocurrent is seen as compared to the dark current. On the other hand at 850 nm, a smaller difference in the dark and photocurrents is observed relative to 505 nm. The results show that the Ni/CuO/Ni device exhibits enhanced photodetection properties at 505 nm wavelength whose energy is slightly above the band gap energy of copper oxide film. The CuO semiconductor absorbs this energy which results in the excitation of electrons from the valence

band to the conduction band, thus leaving behind a hole. The free carriers, generated in this way are responsible for increasing the current at 505 nm. However, the photocurrent changes insignificantly at 365 and 405 nm which is because of the high absorption co-efficient of the CuO. Consequently, the semiconductor absorbs light closer to its surface, which causes the recombination of free charge carriers and results in the photocurrent limitation. The photocurrent increases when the device is exposed to infrared light (850 nm). This is most likely due to the free charge carriers' contribution from the silicon substrate. This can be explained by the fact that the CuO film does not absorb the light higher than its band gap wavelength. Thus at this wavelength, the light is absorbed by the silicon to generate free electrons and holes and hence the photocurrent increases.

Fig. 5 shows the current-voltage response of the MSM device under 505 nm light (2.1 mW/cm^2). The figure depicts the Schottky contact between metal and semiconductor in both forward and reversed directions. The formation of Schottky contacts instead of ohmic ones (as predicted theoretically) is ascribed to the Fermi-level pinning at the metal-semiconductor interface [40]. When the Ni (metal) comes in contact with the CuO (semiconductor), then a high density of metal states are formed within the band gap of the semiconductor. Most of these states are located below the Fermi-level and contain a high density of free charge carriers which is transferred from semiconductor to metal. As a result, the Fermi-level is pinned at the metal-semiconductor interface under

equilibrium and a Schottky contact is formed. The dark current of the device is found to be $3.56 \mu\text{A}$ at 5V whereas the photocurrent at 505 nm increases to $86 \mu\text{A}$ at 5V (Fig. 5). Further, it is noticed that the forward threshold voltage of CuO (1.6V) increases to 2.5V in light exposure. This increase in the threshold voltage is attributed to the recombination of free charge carriers in the presence of light at the lower voltage. Consequently, when the voltage increases, the charge carriers are swept away towards their electrodes, resulting in the generation of photocurrent [35]. The value of the Schottky barrier height for the I-V curve in the dark and the curve under 505 nm light was calculated by using the thermionic emission model. According to this model, the current 'I' can be expressed as follows [41-42];

$$I = I_o \left[\exp\left(\frac{qV}{nkT}\right) - 1 \right] \quad (3)$$

In the above equation, 'I_o' represents saturation current. 'q' is the charge, n is the ideality factor. K is Boltzmann constant and T is the temperature. The saturation current (I_o) can be expressed as;

$$I_o = AA^*T^2 \exp\left(\frac{-q\Phi_B}{kT}\right) \quad (4)$$

Here A* is the effective Richardson constant, 'A' is the activation area, and Φ_B is the Schottky barrier height. The above equation can be expressed to evaluate the Φ_B as follows;

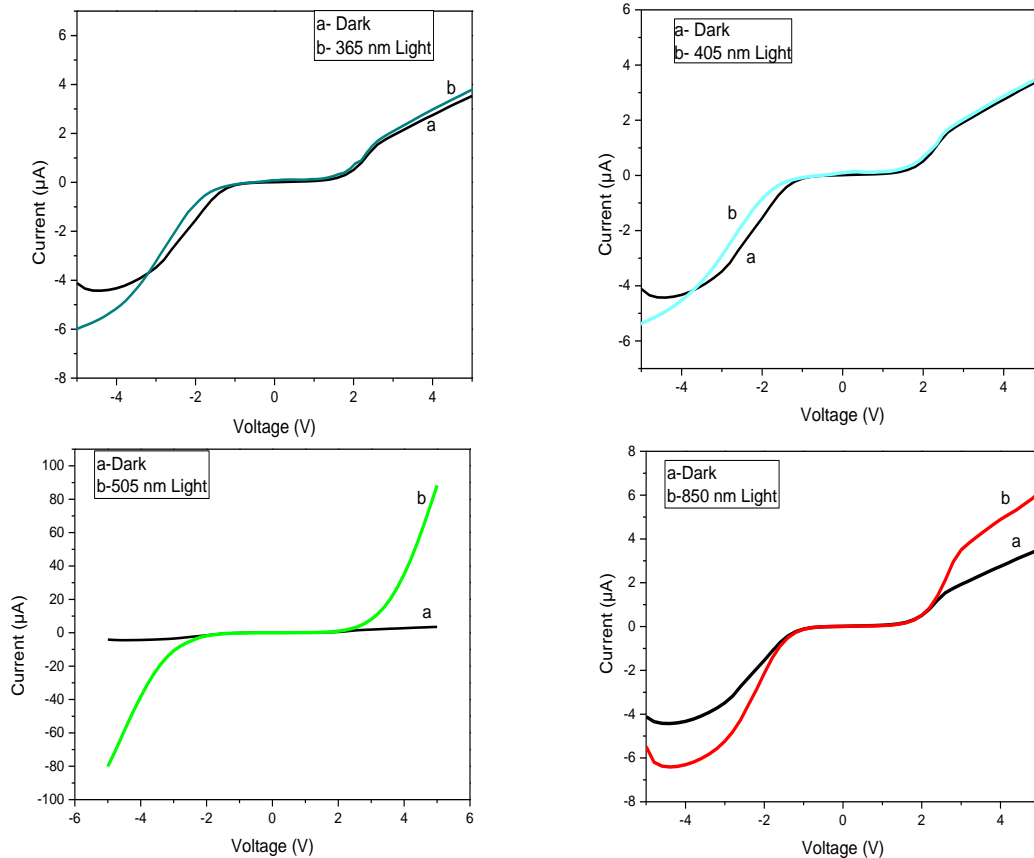


Fig. 5. Current-voltage characteristics of Ni/CuO/Ni photodetector (color online)

$$\Phi_B = \frac{kT}{q} \ln \frac{(AA^* T^2)}{I_0} \quad (5)$$

The A^* value for CuO was taken $110.27 \text{ A.cm}^{-2}.\text{K}^{-2}$ [42], whereas the activation area was 0.080 cm^2 . The values of I and I_0 were taken out from the I-V curve drawn on a semi-logarithmic scale. The Φ_B value was calculated after putting the values of all the parameters in the above equation. The values of Φ_B in the dark and in 505 nm light are found to be 0.832 and 0.814 eV, respectively. The decrease in barrier height at 505 nm light exposure is due to the increase in the photocurrent because of the generation of free electrons and holes. This is caused by the molecular re-ordering/restructuring of the surface states [43].

The responsivity of fabricated Ni/CuO/Ni photodetector at different light wavelengths by using the following equation;

$$R = \frac{I_p}{EA} \quad (6)$$

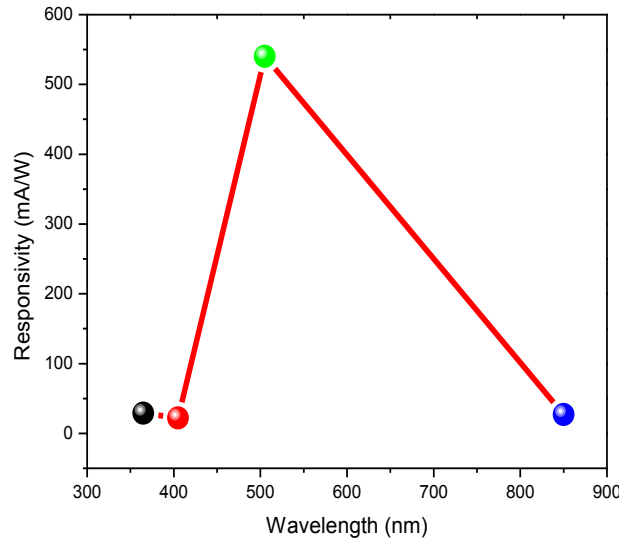


Fig. 6. Spectral response of Ni/CuO/Ni photodetector at different wavelengths (color online)

The current-time measurements were performed on the device at various biased voltages to obtain the device sensitivity and gain. For this purpose, the 2.5 mA/W light was switched OFF and ON repeatedly to observe the rise/decay of current in the voltage range of 2 to 7V. The pulses of current-time obtained at various voltages are shown in Fig 7. The photocurrent increases as the light is switched ON, and then the current reduces to zero when the light is turned OFF. Fig. 7 shows that the current increases under the light with increasing the applied voltage. The current at 7 V is higher than that at the other voltages. This implies that the increase in voltage facilitates the free charge carriers' movement under increased electrical energy and consequently the photocurrent increases. The current gain (G), sensitivity in percentage (%S) can be obtained from the equations mentioned below [35, 44];

$$G = \frac{I_{ph}}{I_d} \quad (7)$$

$$S = \frac{(I_{ph}-I_d)}{I_d} \times 100 \quad (8)$$

Here, E represents light irradiance whose values at 365, 405, 505 and 850 nm were 1.6, 2.1, 2.1 and 2.8 mW/cm². 'A' is the activation area (0.08 cm^2), and I_p is the photocurrent calculated from the I-V graphs at 5 V. The responsivity of the device is drawn against the light wavelength as shown in Fig. 6. The figure shows that the device responsivity is maximum (540 mA/W) at 505 nm, as compared to other wavelengths. This responsivity is higher than that of the CuO based MSM photodetector fabricated with Ag electrodes, reported in a previous study [29]. The high value of responsivity at 505 nm is due to a large number of free charge carriers generated in the semiconductor by the incident light. On the other hand, the low responsivity above 505 nm is due to an increase in the absorption co-efficient of the CuO that results in the recombination of free charge carriers (i.e. electrons and holes).

The G and S (%) in the voltage range of 2 to 7 V, are presented in Table 2. The G and S (%) increase with increasing the applied voltage. The highest G and S values are recorded as 34 and 3200 % when the external biased voltage is at 7V.

The time taken by the current to rise from 10 to 90 % of its value (rise time) was calculated from the magnified current-time graphs. Similarly, the time in which photocurrent decay time from 90 to 10 % (fall time) was also noticed from the graphs in Fig. 6. The rise and fall time values are shown in Table 2, indicating no significant

difference with the change of voltage and it remains almost constant.

The insignificant variation in the rise and fall time can be due to the structural defects inside the film. The rise and fall time values at 7V are 302 and 232 m sec, respectively. The responsivity at different biased voltages was calculated using Eq. (6) and the obtained values are given in Table 2.

Table 2. Photodetection parameters of CuO film based MSM photodetector

V	G	S (%)	t _{rise} (sec)	t _{fall} (sec)	R (mA/W)
2	1.85	85	0.312	0.216	5.8
3	3.07	207	0.262	0.215	46
4	10	280	0.312	0.240	198
5	18	1700	0.296	0.240	540
6	26	2500	0.304	0.240	807
7	34	3200	0.302	0.232	1047

The results of this study are compared with the previously investigated visible light sensitive photodetectors in Table 3. The comparison shows a remarkable performance of the CuO film based

photodetector fabricated in this work. Further improvements can be made in the future by reducing the structural defects in the film.

4. Summary

A monoclinic cupric oxide film is produced by the sputter deposition of copper in a reactive oxygen atmosphere at room temperature. The deposition of Ni on copper oxide film forms Schottky contacts between metal and semiconductor interface which is attributed to Fermi-level pinning effect at the metal-semiconductor interface. The Schottky contact in copper oxide film promotes low dark current. The copper oxide film with a band gap of 2.42 eV shows high sensitivity to 505 nm light and photocurrent is considerably increased. The Ni/CuO/Ni MSM photodetector shows a high current gain, sensitivity and responsivity under green light. The current gain decreases when the device is exposed to either ultraviolet light or infrared light. The current gain and sensitivity are increased with the increase of biased voltage. However, insignificant changes are observed in the rise and fall time of the device with the increase of applied voltage.

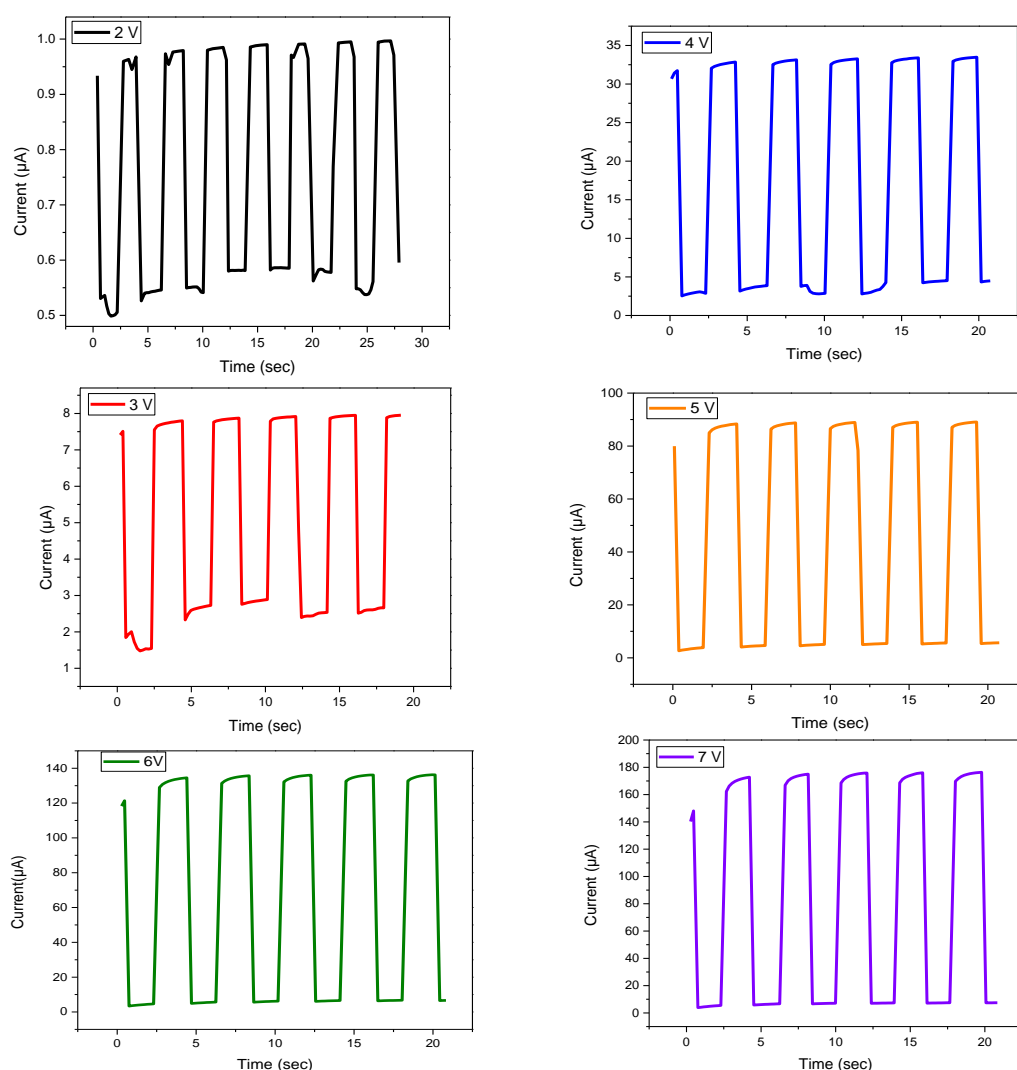


Fig. 7. Current-time characteristics of Ni/CuO/Ni photodetector (color online)

Table 3. Comparison of photodetection parameters of various visible photodetectors

Material type	Substrate type	Fabrication technique	Type of detector	λ (nm)	Bias Voltage (V)	R (A/W)	% S	Rise time (s)	Reference
CuO	Si (100)	DC Magnetron	MSM	505	7	1.04	3.2×10^3	0.302	Present work
CuO	Quartz	Electron beam evaporation	MSM	450	5	0.00033	40.30	53.8	[29]
V ₂ O ₅	Si (100)	Spray Pyrolysis	MSM	540	5	0.94	2.6×10^3	0.700	[45]
CDS	Si (100)	CBD	MSM	500	1	0.24	9.7×10^3	0.009	[46]
ZnO/Cu ₂ O	FTO glass	Hydrothermal/CBD	Heterojunction	425	0	0.0082	--	0.140	[47]
Cu ₂ O/Ag/ZnO	ITO glass	Electrochemical deposition	Heterostructure	564	2	0.27	--	--	[48]
MoS ₂	SiO ₂ /Si	Thermolysis Process	MSM	532	10	0.57	--	7×10^{-5}	[49]
InAlN	Si (111)	Co-Sputtering	MSM	520	5	0.67	4.8×10^3	0.620	[41]
TlInSse	Glass	Bridgman Technique	MSM	532	10	0.61	--	0.300	[50]
ZnO QDs/MoS ₂	Sapphire	CVD/Sol gel	Heterojunction	532	0.5	0.084	--	1.5	[51]

References

- [1] G. Papadimitropoulos, N. Vourdas, V. Em. Vamvakas, D. Davazoglou, *J. Phys. Conf. Series* **10**, 182 (2005).
- [2] V. Figueiredo, E. Elangovan, G. Goncalves, P. Barquinha, L. Pereira, N. Franco, E. Alves, R. Martins, E. Fortunato, *Appl. Surf. Sci.* **254**, 3949 (2008).
- [3] A. S. M Rahman, M. A. Islam, K. M. Shorowordi, *Procedia Eng.* **105**, 679 (2015).
- [4] D. M. Jundale, P. B. Joshi, Shashwati Sen, V. B. Patil, *J. Mater. Sci. Mater. El.* **23**, 1492 (2012).
- [5] E. A. Souza, R. Landers, L. P. Cardoso, Tersio G. S. Cruz, M. H. Tabacniks, A. Gorenstein, *J. Power Sources* **155**, 358 (2006).
- [6] Y. F. Lim, C. S. Chua, C. J. J. Lee, D. Chi, *Phys. Chem. Phys.* **16**, 25928 (2014).
- [7] P. Samarasekara, N. T. R. N Kumara, N. U. S. Yapa, *J. Phys. Condens. Mater.* **18**, 2417 (2006).
- [8] W. Zheng, Y. Chen, X. Peng, K. Zhong, Y. Lin, Z. Huang, *Mater.* **11**, 1253 (2018).
- [9] B. Balamurugan, B. R. Mehta, *Thin Solid Films* **396**, 90 (2001).
- [10] T. H. Darma, A. A. Ogwu, F. Placido, *Mater. Tech.* **26**, 28 (2013).
- [11] S. Eisermann, A. Kronenberger, A. Laufer, J. Bieber, G. Haas, S. Lautenschlager, G. Homm, P. J. Klar, B. K. Meyer, *Phys. Status Solidi A* **209**, 531 (2012).
- [12] M. Muhibbullah, M. Ichimura, *Jpn. J. Appl. Phys.* **49**, 081102 (2010).
- [13] Ang Li, Huaihe Song, Wenbo Wan, Jisheng Zhou, Xiaohong Chen, *Electrochim. Acta* **132**, 42 (2014).
- [14] M. Dhaouadi, M. Jlassi, I. Sta, I. B. Miled, G. Mousdis, M. Kompitsas, W. Dimassi, *Am. J. Phys. Appl.* **6**, 43 (2018).
- [15] D. Osorio-Rivera, G. Torres-Delgado, J. Márquez-Marín, R. Castanedo-Pérez, M. A. Aguilar-Frutis, O. Zelaya-Ángel, *J. Mater. Sci. Mater. El.* **29**, 851 (2018).
- [16] M. Majumder, I. Biswas, S. Pujaru, A. K. Chakraborty, *Thin Solid Films* **589**, 741 (2015).
- [17] D. Prasanth, K.P. Sibin, Harish C. Barshilia, *Thin Solid Films* **673**, 78 (2019).
- [18] K. Saha, A. Bishta, S. A. Khanb, A. Pandey, S. Mohapatra, *Ceram Int.* **46**, 7499 (2020).
- [19] A. Dulmaa, H. Vrielinck, S. Khelifi, Diederik Depla, *Appl. Surf. Sci.* **492**, 711 (2019).
- [20] W. Li, *Surf. Rev. Lett.*, **25**, 1850051 (2018)
- [21] S. Sai Guru Srinivasan, B. Govardhanan, P. Aabel, M. Ashok, M. C. Santhosh Kumar, *Sol. Energy* **187**, 368 (2019).
- [22] S. K. Kumar, S. Murugesan, S. Suresh, S.P. Raj, *J. Sol. Energy*, Article ID 147270 (2013).
- [23] Q. Zhang, K. Zhang, D. Xu, G. Yang, H. Huang, F. Nie, C. Liu, S. Yang, *Prog. Mater. Sci.* **60**, 208 (2014).
- [24] H. J. Song, M. H. Seo, K. W. Choi, M. S. Jo, J. Y. Yoo, J. B. Yoon, *Sci. Rep.* **9**, 7334 (2019).
- [25] R. R. Prabhu, A. C. Saritha, M. R. Shijeesh, M. K. Jayaraj, *Mater. Sci. Engg. B* **220**, 82 (2017).
- [26] J. Sultana, A. Bhattacharya, A. Karamakar, G. K. Dalpati, S. Chattopadhyay, *J. Mater. Sci.* **42**, 194 (2019).
- [27] K. Zhang, M. Peng, W. Wu, J. Guo, G. Gao, Y. Liu, J. Kou, R. Wen, Y. Lei, A. Yu, Z. Zhang, J. Zhai, J. Zhai, Z. L. Wang, *Mater. Horizons* **4**, 274 (2017).
- [28] S. I. Inamdar, K.Y. Rajpure, *J. Alloys Compd.* **595**, 55 (2014).
- [29] P. V. Raghavendra, J. S. Bhat, N. G. Deshpande, *Superlattice Microst.* **113**, 754 (2018).
- [30] P. K. Ooi, C. G. Ching, M. A. Ahmad, S. S. Ng, M. J. Abdullah, H. A. Hassan, Z. Hassan, *Sains Malaysiana* **43**, 617 (2014).
- [31] Anas A. Ahmed, N. Afzal, M. Devarajan, S. Subramani, *Mater. Res. Express* **3**, 116405 (2016).
- [32] B. A. Bhat, G. R. Khan, K. Asokan, *RSC Adv.* **5**, 52602 (2015).
- [33] P. S. Shewale, Y. S. Yu, *J. Alloys Compd.* **654**, 79 (2016).
- [34] D. Kim, J. Y. Leem, *Scientific Reports* **11**, 382 (2021).
- [35] H. Ahmad, N. Afzal, M. Rafique, A. A. Ahmed, R. Ahmed, Z. Khaliq, *Ceram Int.* **46**, 20477 (2020).
- [36] R. Younas, N. Afzal, M. Rafique, M. Imran, M. Saleem, R. Ahmad, *Ceram Int.* **45**, 15547 (2019).
- [37] A. A. Ahmed, M. Devarajan, N. Afzal, *Semicond. Proc.* **63**, 137 (2017).

- [38] L. A. Dahonog, M. S. D. C. Dela Vega, M. D. L. Balela, IOP Conf. Series: J. Phys. Conf. Ser. **1191**, 012043 (2019).
- [39] M. A. Rafea, N. Roushdy, J. Phys. D: Appl. Phys. **42**, 015413 (2009).
- [40] Y. Liu, J. Guo, E. Zho, L.Liao, S. J. Lee, M. Ding, I. Shakir, V. Gambin, Y. Huang, X.F. Duan, Nature **557**, 696 (2018).
- [41] N. Afzal, M. Devarajan, Eur. Phys. J. Appl. Phys. **76**, 10101-1-8 (2016).
- [42] R. Jana, S. Sil, A. Dey, J. Datta, P. P. Ray, AIP Adv. **8**, 125104 (2018).
- [43] H. E. Lapa, A. Kokce, D. A. Aldemir, A. F. Ozdemir, S. Altindal, Indian J. Phys. **94**, 1921 (2019).
- [44] A. A. Ahmed, M. Devarajan, N. Afzal, Sens. Actuators A **262**, 78 (2017).
- [45] N. M. Abd-Alghafour, Naser. M. Ahmedb, Z. Hassan, Sens. Actuators A **250**, 250 (2016).
- [46] M. Husham, Z. Hassan, Abass M. Selman, Eur. Phys. J. Appl. Phys. **74**, 10101 (2016).
- [47] Z. Bai, Y. Zhang, J. Alloys Compd. **675**, 325 (2016).
- [48] W. Li, D. Wang, Z. Zhang, X. Chu, X. Feng, X. Wang, D. Fang, F. Lin, X. Wang, Z. Wei, Optical Mater. Express **8**, 3561 (2018).
- [49] D. S. Tsai, K. Ku Liu, D. H. Lien, M. L. Tsai, C. F. Kang, C. A. Lin, L. J. Li, J. H. He, ACS Nano **7**, 3905 (2013).
- [50] M. T. Khan, I. M. Ashraf, A. Wahab, M. F. Sanaa, M. S. Awad, A. Juman, A. Almohammed, M. Shakir, S. AlFaify, Phys. Scr. **94**, 105816 (2019).
- [51] Y. H. Zhou, Z. B. Zhang, P. Xu, H. Zhang, B. Wang, Nanoscale Res. Lett. **14**, 364 (2019).

*Corresponding author: Naveed.phys@gmail.com